Author Manuscript

Author Manuscript

Author Manuscript

Author Manuscript

HHS Public Access

Author manuscript

J Neuroimaging. Author manuscript; available in PMC 2023 January 01.

Published in final edited form as:

J Neuroimaging. 2022 January ; 32(1): 141–147. doi:10.1111/jon.12923.

Global cerebrospinal fluid as a zero-reference regularization for brain quantitative susceptibility mapping

Alexey V. Dimov[1], **Thanh D. Nguyen**[1], **Pascal Spincemaille**[1], **Elizabeth M. Sweeney**[2], **Nicole Zinger**[3], **Ilhami Kovanlikaya**[1], **Brian H. Kopell**[4], **Susan A. Gauthier**[3], **Yi Wang**[1]

[1]Department of Radiology, Weill Cornell Medicine, New York, USA

[2]Department of Population Health Sciences, Weill Cornell Medicine, New York, USA

[3]Department of Neurology, Weill Cornell Medicine, New York, USA

[4]Nash Family Center for Advanced Circuit Therapeutics, Icahn School of Medicine at Mount Sinai, New York, USA

Abstract

Background and Purpose: The objective ofthis study was to demonstrate a global cerebrospinal fluid (CSF) method for a consistent and automated zero referencing of brain quantitative susceptibility mapping (QSM).

Methods: Whole brain CSF mask was automatically segmented by thresholding the gradient echo transverse relaxation (R_2^*) map, and regularization was employed to enforce uniform susceptibility distribution within the CSF volume in the field-to-susceptibility inversion. This global CSF regularization method was compared with a prior ventricular CSF regularization. Both reconstruction methods were compared in a repeatability study of 12 healthy subjects using *t*-test on susceptibility measurements, and in patient studies of 17 multiple sclerosis (MS) and 10 Parkinson's disease (PD) patients using Wilcoxon rank-sum test on radiological scores.

Results: In scan-rescan experiments, global CSF regularization provided more consistent CSF volume as well as higher repeatability of QSM measurements than ventricular CSF regularization with a smaller bias: –2.7 parts per billion (ppb) versus –0.13 ppb (*t*-test $p<0.05$) and a narrower 95% limits of agreement: [−7.25, 6.99] ppb versus [−16.60, 11.19 ppb] (*f*-test $p<0.05$). In PD and MS patients, global CSF regularization reduced smoothly varying shadow artifacts and significantly improved the QSM quality score ($p<0.001$).

Conclusions: The proposed whole brain CSF method for QSM zero referencing improves repeatability and image quality of brain QSM compared to the ventricular CSF method.

Keywords

artifact reduction; quantitative susceptibility mapping; repeatability; zero referencing

Correspondence Yi Wang, PhD, 407 East 61st St, Suite RR118, New York, NY 10021, USA., yiwang@med.cornell.edu.

Author Manuscript Author Manuscript Author Manuscript Author Manuscript

INTRODUCTION

Quantitative susceptibility mapping (QSM) allows the mapping of magnetic susceptibility sources (e.g., calcium, iron, or contrast agents) in tissue from complex gradient echo MRI data.[1] Zero referencing is an essential component of magnetic susceptibility quantification, because, in QSM, the susceptibility is estimated up to a constant. One possibility is to set the average susceptibility value over the whole brain or cortical gray matter to be zero.[2] However, it has been performed after QSM reconstruction and only in healthy subjects. In patients with neurological diseases, gray matter can be affected by the pathology and care is needed when used for zero referencing. Furthermore, cortical gray matter segmentation is a time-consuming process, and might be impractical. Whole brain referencing might also provide suboptimal results, as many pathologies can change average susceptibility of the brain through accumulation of iron, demyelination, gray matter atrophy, and so on. Alternatively, cerebrospinal fluid (CSF) with its chemical resemblance to pure water could be viewed as a natural zero reference.[3–7] However, nonuniformity of QSM is observed within the ventricular CSF in healthy subjects and patients alike using conventional dipole inversion algorithms.[8] This is artifactual and can be suppressed using an L_2 regularization in QSM reconstruction as in the morphology enabled dipole inversion with automatic uniform CSF zero-reference (MEDI+0) algorithm.[8]

Recently, there has been an increasing interest in the application of QSM to the cross-sectional and longitudinal tracking of progression of various diseases, which makes the zero referencing even more critical since variable global shifts between different scans can complicate the analysis of the results.[9–19] However, separate data acquisitions inevitably introduce unwanted variations in subject's head orientation within the scanner, location of the imaging volume, imaging resolution, among others. These factors influence the heterogeneity of the magnetic field and the corresponding R_2^* map.[20,21] As the R_2^* map is used for the ventricle CSF segmentation in MEDI+0, these variations can cause fluctuations in ventricle segmentations, resulting in inconsistent QSM referencing that may introduce unwanted variability in intrasubject or intersubject susceptibility measurements. Therefore, it is highly desired to improve CSF segmentation for reliable QSM zero referencing.

In this work, we present a global CSF method for a consistent and automated zero referencing of QSM through inclusion of all CSF spaces across the brain. Furthermore, we demonstrate that the proposed technique brings about additional image quality improvements.

METHODS

Ventricular and global CSF regularization

The previously proposed MEDI+0 approach extends the original MEDI formulation by introducing CSF zero referencing during QSM reconstruction. It is formulated as the following minimization problem:[8,22]

Author Manuscript Author Manuscript Author Manuscript Author Manuscript

$$\overline{\chi} = argmin_{\chi} \frac{1}{2} \left\| w\left(e^{-if} - e^{-i(d * \chi)}\right) \right\|_2^2 + \lambda_1 \| M_G \nabla \chi \|_1 + \lambda_2 \left\| M_{CSF}^V (\chi - \overline{\chi_{CSF}}) \right\|_2^2 \quad (1)$$

$$\chi * = \tilde{\chi} - \overline{\tilde{\chi}_{CSF}}$$

Here, χ^* is the sought-after susceptibility map, d is the dipole kernel, w is the acquisition noise weighting, f is the input local field, M_G represents the morphological prior in the form of a binary edge mask derived from the magnitude image, M_{CSF}^V is a mask of the ventricular CSF, $\overline{\chi_{CSF}}$ is the operator computing the average over the mask M_{CSF}^V, and λ_1 and λ_2 are regularization parameters. The third term in Equation (1) enforces uniform susceptibility distribution within the CSF region.

In its original implementation, MEDI+0 considered only ventricular CSF region for regularization purposes. Accordingly, the algorithm included thresholding of the gradient echo transverse relaxation (R_2^*) map and connectivity-based filtering, which, due to noise, partial voxel effects, and dependence of R_2^* on orientation of patient's head relative to B_0 direction, can result in an inconsistent segmentation M_{CSF}^V between acquisitions performed in the same subject (Figure 1). Because the zero reference is based on the average susceptibility within M_{CSF}^V, this inconsistency may introduce an undesirable global shift of brain susceptibility values in both inter and intrasubject comparison. To address these shortcomings, we propose to utilize a global CSF regularization based on a simple thresholding of the R_2^* map.

Human subject studies

The imaging studies were approved by the local Institutional Review Board and informed consents were obtained from all subjects. Twelve healthy subjects (five males, seven females, mean age 26.8 years ± 4.1) were imaged in two consecutive MRI sessions using the same acquisition protocol on a 3T scanner (Siemens Prisma, VE11B). Between the two scanning sessions, the subjects were asked to sit up and lie down again to mimic head repositioning in an actual MRI examination. The acquisition protocol included a 1 mm isotropic T1-weighted (T1W) Magnetization Prepared Rapid Acquisition Gradient Echo sequence for structural imaging with acquisition parameters TI=900 ms, TR=2300 ms, FA=8°; and a multi-echo gradient echo sequence (mGRE) for QSM with TE1/ΔTE = 6.3/4.06 ms TR=48 ms, FA=15°, voxel size = 0.8 mm×0.8 mm×3 mm, matrix size = 260×320×56. R_2^* maps were calculated from the mGRE magnitude image using the ARLO method.[23] A brain mask was obtained from the echo-combined mGRE magnitude image using FSL BET algorithm.[24] As in the original MEDI+0 implementation, global CSF mask M_{CSF}^G was obtained by selecting all voxels within the brain mask whose R_2^* was at or below 5 Hz.[8] The ventricular CSF mask M_{CSF}^V was then computed: first, brain centroid was specified based on the brain mask, a central brain region with the radius of 3 cm

Author Manuscript Author Manuscript Author Manuscript Author Manuscript

was defined, and three largest components of M_{CSF}^{G} overlapping with this region were selected to form M_{CSF}^{V}. Sixteen subcortical regions of interest (ROIs)—frontal white matter (WM), parietal WM, temporal WM, occipital WM, thalamus, caudate nucleus, putamen, and pallidum in both hemispheres—were automatically segmented on the T1W image using FreeSurfer and coregistered onto the mGRE image using FSL FLIRT algorithm.[25,26] Brain susceptibility maps were reconstructed for each scan and each CSF reference mask. Regularization parameters were fixed for both methods with the following values: λ_1 = 1000 and λ_2 = 60. Repeatability of the susceptibility values estimated using the two CSF reference masks were compared using Bland–Altman analysis and *t*-test. Additionally, global CSF mean and standard deviations, as well as scan-rescan differences in volumes of segmented regularization ROIs, were recorded for both reconstruction methods.

To assess the effects of MEDI+0 regularization type in clinical data acquired with different imaging protocols, QSMs from anonymized brain MGRE data acquired in 17 multiple sclerosis (MS) patients and 10 Parkinson's disease (PD) patients acquired at 3T (GE Healthcare, Milwaukee, WI) were retrospectively reconstructed using both the ventricular and global CSF regularization. The QSM acquisition parameters were: for MS, TE1/ΔTE/nTE = 4.5/4.8 ms/11, TR=57.3 ms, FA=15°, voxel size = 0.8 mm×0.8 mm×3 mm; for PD, TE1/ΔTE/nTE = 4.2/4.9 ms/10, TR=53.9 ms, FA=15°, acquired voxel size = 0.5 mm×0.5 mm×0.5 mm. Regularization parameters were fixed for both methods with the following values: λ_1 = 1000 and λ_2 = 60 for MS data and λ_1 = 2500 and λ_2 = 60 for PD data. A neuroradiologist (I. K., 20 years of experience) reviewed both QSM reconstructions from each subject and scored the relative QSM image quality using a 3-point scale (1=better, 0=same, and −1=worse) for each of the following criteria: presence of artifacts, such as shadowing and streaking in QSM maps, gray/WM differentiation, lesion conspicuity, appearance of venous structures, and CSF in the ventricles. A Wilcoxon rank-sum test was employed to test the difference between the two imaging methods. In all statistical tests, the level of significance was chosen to be 0.05.

RESULTS

Scan-rescan quantitative susceptibility mapping

In healthy volunteers, the volume of the M_{CSF} segmented for ventricular CSF regularization was 6.8±7.8 cm^3, while that for global CSF segmentation was 20.4±13.2 cm^3 (p<0.05). For ventricular CSF regularized QSMs, Bland–Altman plots showed a bias of −2.7 ppb with 95% limits of agreement of [−16.60, 11.19] ppb between the repeated scans. The application of global CSF regularization reduced the bias to −0.13 ppb (*t*-test p<0.05) and narrowed the 95% limits of agreement to [−7.25, 6.99] ppb (*t*-test p<0.05) (Figure 2). For ventricular CSF regularization, the average relative interscan difference between CSF regularization volumes was 14% compared to 3% for the global CSF regularization (p = 0.06), with the absolute volume difference 0.64±0.68 cm^3 and 0.6±0.47 cm^3 (p=0.94), respectively. Figure 3 demonstrates an example with significant change in the segmented ventricular CSF volume between the test and retest scans, which is not present in the proposed global CSF segmentation approach.

Author Manuscript Author Manuscript Author Manuscript Author Manuscript

Single timepoint QSM imaging

The volume of the ventricular CSF mask M_{CSF}^{V} in the MS patient cohort was 18±18 cm^3, while that of the global CSF Mask M_{CSF}^{G} was 41±28 cm^3 (p<0.05). In the healthy cohort, the ventricular CSF regularization resulted in an average standard deviation of 35 ppb within M_{CSF}^{G} and an average mean susceptibility of −8 ppb, while the application of the global CSF regularization reduced the average standard deviation of susceptibility within M_{CSF}^{G} to 12 ppb (p<0.05) and its average mean susceptibility to 0 ppb (p<0.05). Similarly, in the MS patient cohort, the ventricular CSF regularization resulted in an average standard deviation of 35 ppb within M_{CSF}^{G} and an average mean CSF susceptibility of −18 ppb; the application of global CSF reduced the average standard deviation to 13 ppb (p<0.05) and average to 0 ppb (p<0.05).

Radiological assessment revealed QSM image quality improvement in 16 out of 17 MS patients when using global CSF regularization (Wilcoxon test p<0.001), with one case being a tie. No difference was observed in terms of the overall gray/WM differentiation, lesion conspicuity, and appearance of venous structures and ventricular CSF. In the MS patients, the proposed regularization led to observable reduction of shadow artifact in the frontal lobe, primarily within prefrontal and motor cortices. Similarly, for the PD patients, shadow artifact reduction for global CSF regularization was observed in 9 out of 10 patients, with one case being a tie (Wilcoxon test p=0.004). No difference was observed in terms of the overall gray/WM differentiation, lesion conspicuity, and appearance of venous structures and ventricular CSF. QSM image quality improvement was reported for sulci, top of frontal and parietal lobes, and around the sagittal sinus.

Figure 4 shows an R_2^* map, segmented CSF masks, and QSM reconstructions for two regularization methods in two axial locations in one MS patient. The proposed global CSF regularization procedure, in addition to the ventricular CSF, incorporates the CSF within the sulci. Consequently, homogeneity of CSF throughout the brain was greatly improved, while susceptibility of other structures (deep gray matter structures and blood vessels) was not affected. Figure 5 shows a comparison of the two QSM reconstructions in a PD patient. Spatially smooth shadow artifacts were noticeably suppressed when using global CSF regularization.

DISCUSSION

In this work, we propose an extension of the previously published MEDI+0 technique which uses L2 regularization of ventricular CSF for calculation of a zero-referenced QSM. Our data demonstrate that through consistent CSF masking, global CSF regularization leads to improved QSM scan-rescan repeatibility in healthy subjects compared to ventricular CSF regularization. Furthermore, the proposed global CSF regularization was found to significantly improve overall image quality and reduce nonlocal shadow artifacts at the brain periphery. Thus, we conclude that global CSF regularization enhances consistent zero referencing, making QSM more suitable for longitudinal studies.

Author Manuscript Author Manuscript Author Manuscript Author Manuscript

In the original work introducing ventricle CSF zero-referenced QSM, the authors based the CSF mask segmentation on "binning" of the R_2^* map that can be estimated from the same GRE data and thus naturally coregistered to QSM. CSF being almost a pure water has very low relaxation rate.[8] In the current study, most of the cerebral CSF volume was found by selecting all those voxels whose R_2^* fell within [0...5] s^{-1}. Nevertheless, the original MEDI+0 implementation only included ventricular CSF to regularize the QSM inversion process. This ventricle CSF approach has been shown to have good performance. However, its repeatability has not been analyzed.[8] Our results here confirm that ventricle segmentation from R_2^* map is prone to variations in data acquisition, which include dependence of R_2^* on orientation of an object relative to B_0 and noise in the data affect accuracy of the morphological filtering.[20] Thus, selection of the predetermined number of connected components is demonstrated to produce variable results within the same subject in a scan-rescan experiment even if the same imaging parameters are used.[8] Consequently, the value of the CSF regularization term in Equation (1) might differ noticeably between acquisitions, changing convergence of the whole minimization problem, as well as changing the average of the solution over the CSF regularization volume. Utilizing global CSF regularization, we demonstrate higher reproducibility of the regularization volume and significantly improved repeatability of the susceptibility measurements in scan-rescan experiment performed in healthy subjects. With this, we conclude that the ventricle segmentation is unnecessary for zero referencing and can be dropped from QSM reconstruction.

The use of the entire CSF space throughout the brain, as demonstrated here, also significantly increases the number of voxels within the regularization volume. This increased spatial coverage in the global CSF regularization is distributed over the entire brain, as CSF does. This large spatial extend over the entire brain provides a means to reduce the shadowing artifacts that arise from the incomplete elimination of the strong background field in the vicinity of air–bone–tissue interface and spread in large scale over the whole brain. By enforcing uniformity (of zero) over the global CSF volume, the global CSF regulation advantageously suppresses this shadowing artifact, leading to improved QSM image quality as demonstrated through the analysis of the radiological impression and comparison of standard deviation of CSF susceptibility in both global and ventricular CSF QSM reconstructions.

The regularization approach presented in our work has one potential methodological limitation. Certain pathological conditions, such as intraventricular hemorrhage or CNS infections (e.g., meningitis and encephalitis), could alter chemical composition of the CSF, rendering its magnetic susceptibility inhomogeneous or different from that of pure water.[27,28] It could be speculated that affected regions of CSF will also experience increase of R_2^* and, as such, may be excluded from the regularization volume; however, this aspect has not been studied. Since performance of the CSF regularization in the presence of CSF-altering pathologies has not been analyzed, caution must be taken for cohorts of subjects where these conditions are present.

In this study, the repeatability analysis was limited to healthy volunteers. A comprehensive reproducibility over different scanners should also be performed.[29] The present range

Author Manuscript Author Manuscript Author Manuscript Author Manuscript

of [0...5] s^{-1} is empirically determined and cannot guarantee complete coverage of the cerebral CSF. For field strengths other than 3T, additional adjustments of this range will be required, as R_2^* scales approximately linearly with field strength. Furthermore, M_{CSF} might be not the only regularizable volume according to the physiological distribution of isotropic susceptibility sources in human brain. Other tissues (e.g., normal cortical gray matter) should be considered for further expansion of the minimization problem described by Equation (1).[2]

ACKNOWLEDGMENTS AND DISCLOSURE

Materials of this publications were in part presented at the ISMRM 2021 annual meeting (program number 4001). Alexey Dimov, Yi Wang, and Pascal Spincemaille are inventors of QSM-related patents issued to Cornell University. Yi Wang and Pascal Spincemaille hold equity in Medimagemetric LLC. Susan Gauthier receives grant support from Genzyme and Genentech. Brian Kopell receives consulting fees from Medtronic, Abbott, and ClearPoint Neuro. The remaining authors declare that they have no disclosures.

Funding information

This work was supported in part by the NIH R01NS105144, R01NS095562, R21AG067466, and S10OD021782

REFERENCES

1. De Rochefort L, Liu T, Kressler B, Liu J, Spincemaille P, Lebon V, et al. Quantitative susceptibility map reconstruction from MR phase data using Bayesian regularization: validation and application to brain imaging. Magn Reson Med 2010;63:194–206. [PubMed: 19953507]
2. Feng X, Deistung A, Reichenbach JR. Quantitative susceptibility mapping (QSM) and R2* in the human brain at 3T: evaluation of intrascanner repeatability. Z Med Phys 2018;28:36–48. [PubMed: 28601374]
3. Wang Y, Liu T. Quantitative susceptibility mapping (QSM): decoding MRI data for a tissue magnetic biomarker. Magn Reson Med 2015;73:82–101. [PubMed: 25044035]
4. Kee Y, Liu Z, Zhou L, Dimov A, Cho J, de Rochefort L, et al. Quantitative susceptibility mapping (QSM) algorithms: mathematical rationale and computational implementations. IEEE Trans Biomed Eng 2017;64:2531–45. [PubMed: 28885147]
5. Khasawneh AH, Garling RJ, Harris CA. Cerebrospinal fluid circulation: what do we know and how do we know it? Brain Circ 2018;4:14–8. [PubMed: 30276331]
6. Bulat M, Klarica M. Recent insights into a new hydrodynamics of the cerebrospinal fluid. Brain Res Rev 2011;65:99–112. [PubMed: 20817024]
7. Straub S, Schneider TM, Emmerich J, Freitag MT, Ziener CH, Schlemmer H-P, et al. Suitable reference tissues for quantitative susceptibility mapping of the brain. Magn Reson Med 2017;78:204–14. [PubMed: 27529579]
8. Liu Z, Spincemaille P, Yao Y, Zhang Y, Wang Y. MEDI+0: morphology enabled dipole inversion with automatic uniform cerebrospinal fluid zero reference for quantitative susceptibility mapping. Magn Reson Med 2018;79:2795–803. [PubMed: 29023982]
9. Bilgic B, Pfefferbaum A, Rohlfing T, Sullivan EV, Adalsteinsson E. MRI estimates of brain iron concentration in normal aging using quantitative susceptibility mapping. Neuroimage 2012;59:2625–35. [PubMed: 21925274]
10. Schweser F, Sommer K, Deistung A, Reichenbach JR. Quantitative susceptibility mapping for investigating subtle susceptibility variations in the human brain. Neuroimage 2012;62:2083–100. [PubMed: 22659482]
11. Deistung A, Schweser F, Wiestler B, Abello M, Roethke M, Sahm F, et al. Quantitative susceptibility mapping differentiates between blood depositions and calcifications in patients with glioblastoma. PLoS One 2013;8:e57924. [PubMed: 23555565]

Author Manuscript Author Manuscript Author Manuscript Author Manuscript

12. Lim IAL, Faria AV, Li X, Hsu JTC, Airan RD, Mori S, et al. Human brain atlas for automated region of interest selection in quantitative susceptibility mapping: application to determine iron content in deep gray matter structures. Neuroimage 2013;82:449–69. [PubMed: 23769915]
13. Langkammer C, Liu T, Khalil M, Enzinger C, Jehna M, Fuchs S, et al. Quantitative susceptibility mapping in multiple sclerosis. Radiology 2013;267:551–9. [PubMed: 23315661]
14. Acosta-Cabronero J, Williams GB, Cardenas-Blanco A, Arnold RJ, Lupson V, Nestor PJ. In vivo quantitative susceptibility mapping (QSM) in Alzheimer's disease. PLoS One 2013;8:e81093. [PubMed: 24278382]
15. Li W, Wu B, Batrachenko A, Bancroft-Wu V, Morey RA, Shashi V, et al. Differential developmental trajectories of magnetic susceptibility in human brain gray and white matter over the lifespan. Hum Brain Mapp 2014;35:2698–713. [PubMed: 24038837]
16. Persson N, Wu J, Zhang Q, Liu T, Shen J, Bao R, et al. Age and sex related differences in subcortical brain iron concentrations among healthy adults. Neuroimage 2015;122:385–98. [PubMed: 26216277]
17. Zhang Y, Gauthier SA, Gupta A, Comunale J, Chia-Yi Chiang G, Zhou D, et al. Longitudinal change in magnetic susceptibility of new enhanced multiple sclerosis (MS) lesions measured on serial quantitative susceptibility mapping (QSM). J Magn Reson Imaging 2016;44:426–32. [PubMed: 26800367]
18. Sun H, Klahr AC, Kate M, Gioia LC, Emery DJ, Butcher KS, et al. Quantitative susceptibility mapping for following intracranial hemorrhage. Radiology 2018;288:830–9. [PubMed: 29916778]
19. Eskreis-Winkler S, Zhang Y, Zhang J, Liu Z, Dimov A, Gupta A, et al. The clinical utility of QSM: disease diagnosis, medical management, and surgical planning. NMR Biomed 2017;30.e3668.
20. Li J, Chang S, Liu T, Wang Q, Cui D, Chen X, et al. Reducing the object orientation dependence of susceptibility effects in gradient echo MRI through quantitative susceptibility mapping. Magn Reson Med 2012;68:1563–9 [PubMed: 22851199]
21. Wharton S, Bowtell R. Fiber orientation-dependent white matter contrast in gradient echo MRI. Proc Natl Acad Sci U S A 2012;109:18559–64. [PubMed: 23091011]
22. Liu T, Wisnieff C, Lou M, Chen W, Spincemaille P, Wang Y, et al. Nonlinear formulation of the magnetic field to source relationship for robust quantitative susceptibility mapping. Magn Reson Med 2013;69:467–76. [PubMed: 22488774]
23. Pei M, Nguyen TD, Thimmappa ND, Salustri C, Dong F, Cooper MA, et al. Algorithm for fast monoexponential fitting based on autoregression on linear operations (ARLO) of data. Magn Reson Med 2015;73:843–50. [PubMed: 24664497]
24. Jenkinson M, Pechaud M, Smith S. BET2: MR-based estimation of brain, skull and scalp surfaces. Presented at the 11th Annual Meeting of the Organization for Human Brain Mapping. June 12–16, 2005; Toronto.
25. Fischl B Freesurfer. Neuroimage 2012;62:774–81. [PubMed: 22248573]
26. Jenkinson M, Bannister P, Brady M, Smith S Improved optimization for the robust and accurate linear registration and motion correction of brain images. Neuroimage 2002;17:825–41. [PubMed: 12377157]
27. Shahan B, Choi EY, Nieves G. Cerebrospinal fluid analysis. Am Fam Physician 2021;103:422–8. [PubMed: 33788511]
28. Ellul M, Solomon T. Acute encephalitis — diagnosis and management. Clin Med (Lond) 2018;18:155–9. [PubMed: 29626021]
29. Deh K, Nguyen TD, Eskreis-Winkler S, Prince MR, Spincemaille P, Gauthier S, et al. Reproducibility of quantitative susceptibility mapping in the brain at two field strengths from two vendors. J Magn Reson Imaging 2015;42:1592–600. [PubMed: 25960320]

Author Manuscript Author Manuscript Author Manuscript Author Manuscript

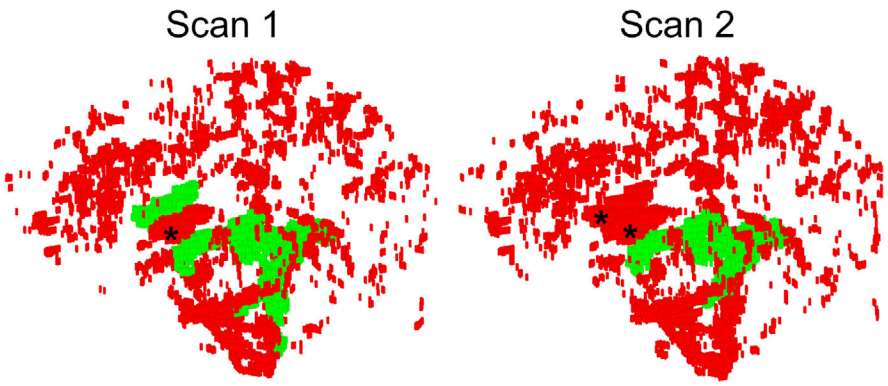

FIGURE 1.

Volumetric rendering of the “global” cerebrospinal fluid (CSF) volume (red) and its overlap with “ventricular CSF” (green) reconstructed from a scan-rescan data of the same healthy volunteer. Note that elimination of the unconnected components in ventricular CSF method resulted in complete erroneous elimination of the anterior horns of lateral ventricles (marked with “*”) in both segmentations, and introduced inconsistent ventricular masking. Furthermore, large volumes of CSF spanning the brain volume are completely discarded during the morphological filtering. While ventricular CSF segmentation demonstrates noticeable variations between scans, the global CSF mask is stable. See Methods for further details

Author Manuscript Author Manuscript Author Manuscript Author Manuscript

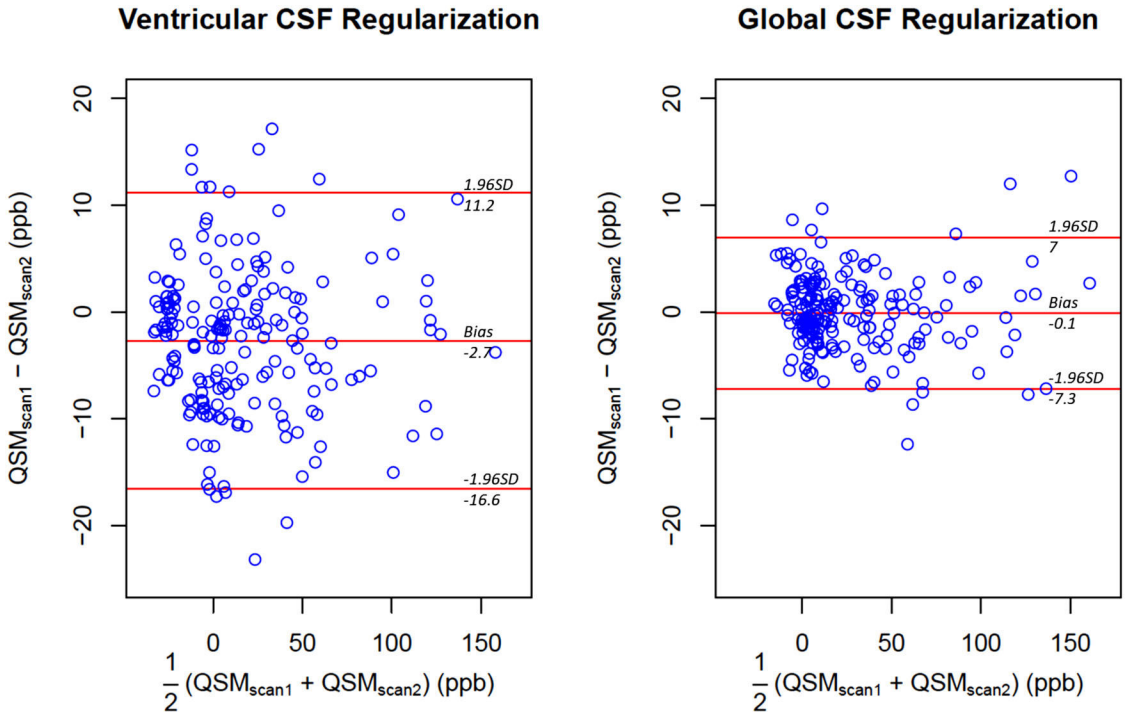

FIGURE 2.

Comparison of the repeatability of regional quantitative susceptibility measurements obtained with ventricular and global cerebrospinal fluid regularization in 16 subcortical regions of interest from 12 healthy subjects. Global cerebrospinal fluid regularization results in negligible bias and narrower 95% limits of agreement of approximately ±7 parts per billion. Abbreviation: SD, standard deviation

Author Manuscript Author Manuscript Author Manuscript Author Manuscript

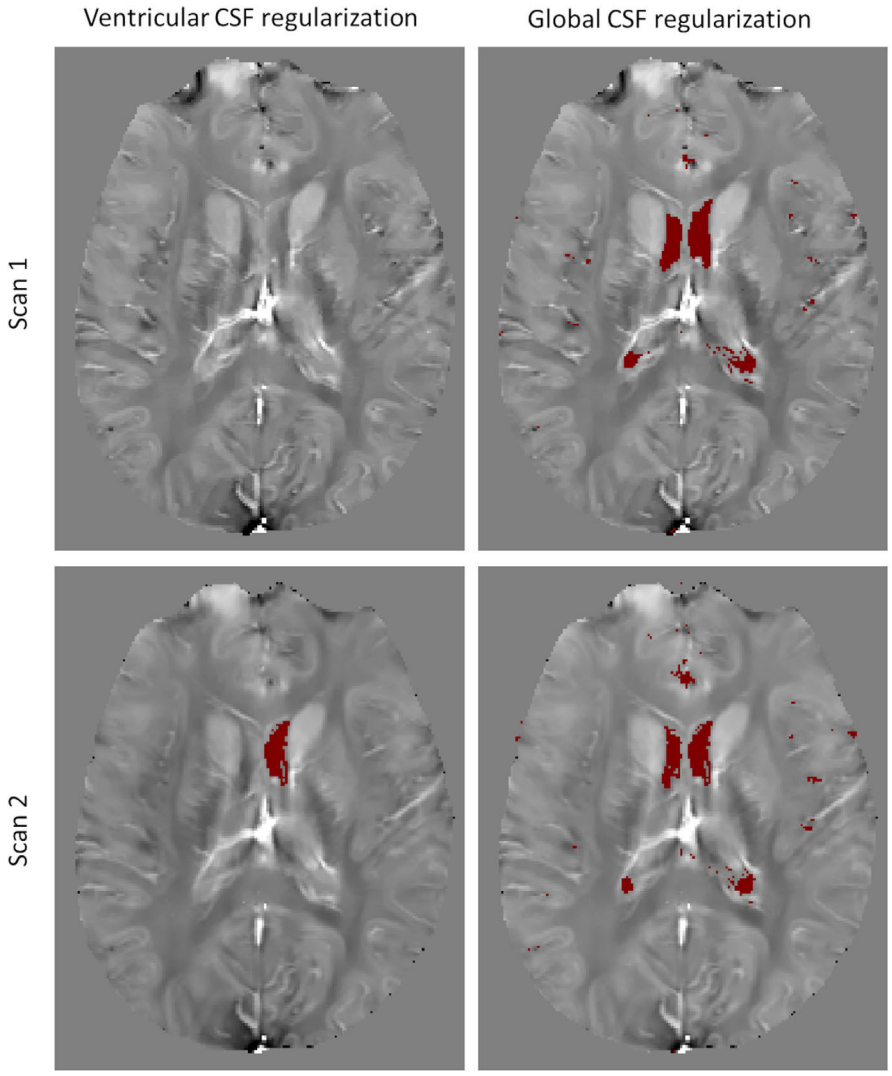

FIGURE 3.

Comparison of consistency of automated segmentation of cerebrospinal fluid masks in ventricular and global regularization methods (same subject as in Figure 1). Elimination of morphological filtering allows more accurate and repeatable segmentation of the regularization volume

Author Manuscript Author Manuscript Author Manuscript Author Manuscript

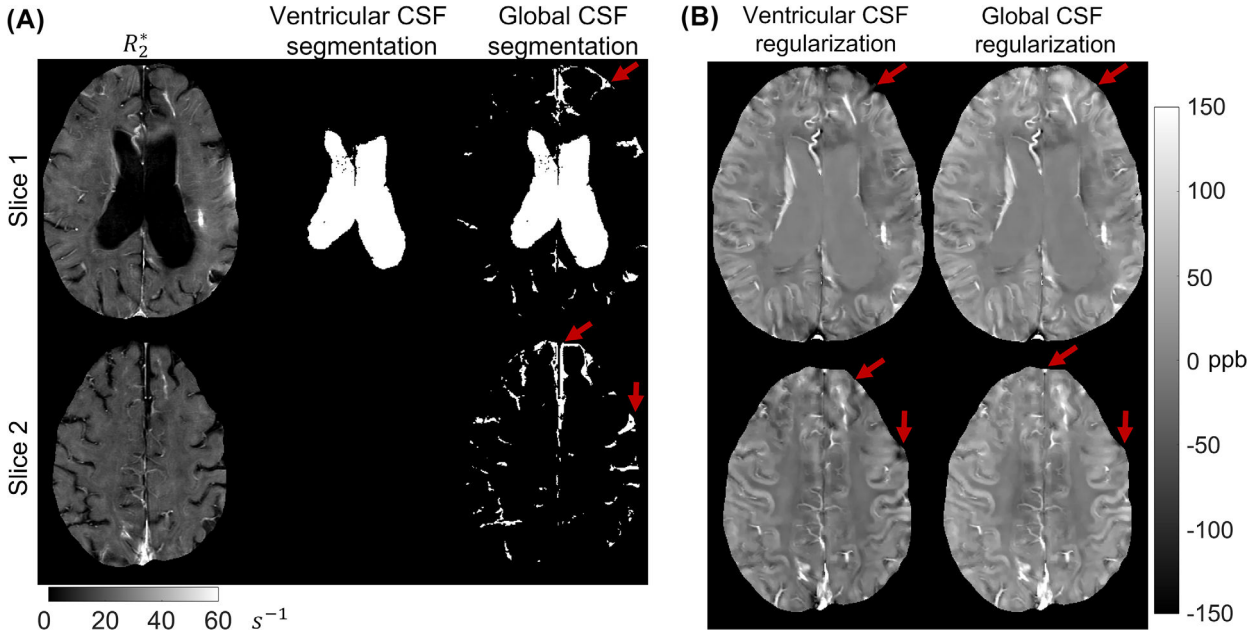

FIGURE 4.

(A) A representative case of a multiple sclerosis patient's segmentation of cerebrospinal fluid for regularization of quantitative susceptibility mapping. Note that the ventricular segmentation method eliminated large volumes of cerebrospinal fluid (CSF) in sulcal space (red arrows) which leads to complete lack of the regularization volumes near the border of the brain. (B) Reconstructed susceptibility maps in this patient. Note the efficient suppression of shadow artifacts at the edge of the brain (red arrows) after the global CSF regularization

Author Manuscript Author Manuscript Author Manuscript Author Manuscript

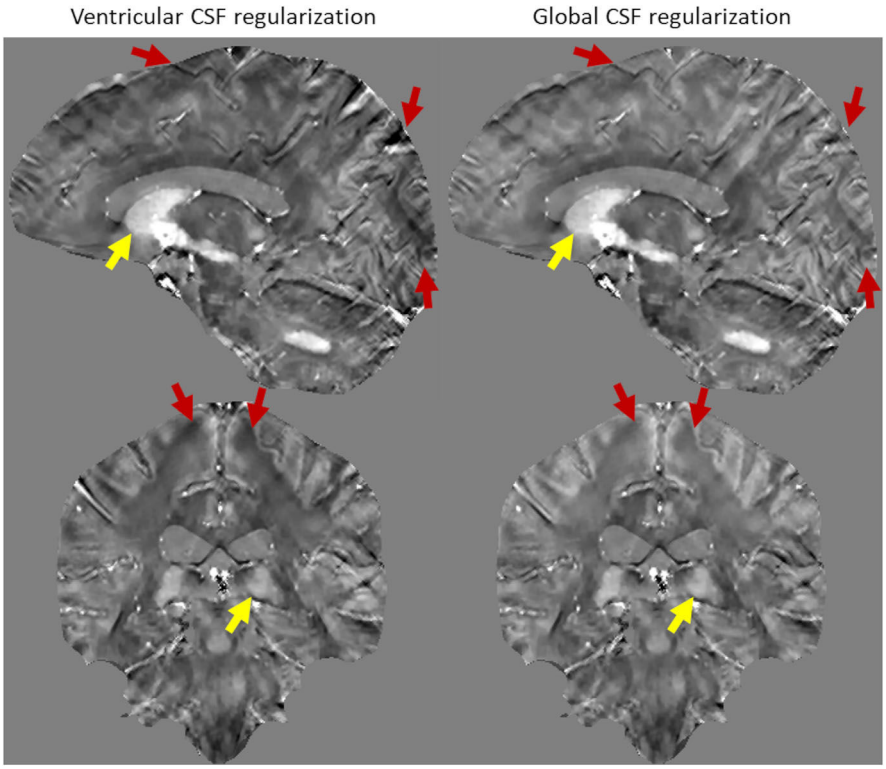

FIGURE 5.

A representative case of a Parkinson's disease patient quantitative susceptibility map (QSM) reconstructed using ventricular and global cerebrospinal fluid (CSF) regularizations. While the QSM values of the deep gray matter structures (yellow arrows) did not change significantly for both reconstructions, global CSF regularization efficiently suppressed spatially smooth shadow artifacts originating at the brain surface (red arrows)